The Role of Pc-5 ULF Waves in the Radiation Belts: Current Understanding and Open Questions

Scot R. Elkington and Theodore E. Sarris

4.1 The role of Pc-5 waves in the radiation belts	80
4.2 Questions: Quantitative determination of transport rates	83
4.3 Conclusions and future possibilities	95
Acknowledgments	96
References	97

■ Abstract

Pc-5 frequency magnetospheric ULF waves have been closely tied to dynamical variations in the energetic electron fluxes observed in the Van Allen radiation belt. The mode of interaction between these global waves and the trapped energetic particles comprising the belts is through a radial transport process that results from breaking of the drift invariant of trapped particle motion, while conserving the bounce and gyro invariants. Most often this is described as a stochastic process, whereby particles being diffusively transported to regions of stronger magnetic field strength increase their energy, while those transported outward to regions of lower magnetic field strength lose energy. In this chapter we describe the properties of ULF waves required to quantitatively determine their effect on radiation belt particles.

4.1 The role of Pc-5 waves in the radiation belts

Variations in the strength and direction of magnetic and electric fields in near-Earth space occur in a wide range of frequencies and plasma wave modes. In particular,

a category of magnetohydrodynamic (MHD) waves known as Pc-5 ULF pulsations (Jacobs et al., 1964) occur at mHz frequencies, and have been established as being strongly correlated with variations in the trapped energetic particle populations that comprise the Van Allen radiation belts (e.g. Baker et al., 1998; Rostoker et al., 1998; Mathie and Mann, 2000; Mann et al., 2004).

In ideal MHD theory a cold plasma will support two basic wave modes: the magnetosonic or compressional wave, and the shear Alfvén wave (e.g. Sturrock, 1994). In their simplest description, the Alfvén mode consists of transverse oscillations propagating parallel to the local magnetic field, while the magnetosonic mode is an isotropically-propagating transverse oscillation. In a cylindrically-symmetric geometry the shear wave is characterized by purely azimuthal magnetic field perturbations, B_{ϕ} , and a radial electric field, E_r , and is commonly referred to as a toroidal-mode Alfvén wave. The compressional wave in this geometry is characterized by oscillations in the total magnetic field strength B_z and an azimuthal electric field E_{ϕ} , and is referred to as a poloidal-mode wave.

ULF waves in the Pc-5 category may be driven either by internal (magnetospheric) plasma processes, or may originate in the dynamic interactions of the Earth's magnetosphere with the solar wind. Internally-generated ULF waves may result from mirror (Hasegawa, 1969) or drift-bounce (Southwood et al., 1969; Chen and Hasegawa, 1991) instabilities, or as a result of anisotropies in the perpendicular ring current (Takahashi et al., 1985). Externally-driven ULF waves may result from shear flow instabilities along the flanks of the magnetopause (Kivelson and Pu, 1984; Cahill and Winckler, 1992; Mann et al., 1999; Claudepierre et al., 2008), as a result of variations in solar wind pressure (Kivelson and Southwood, 1988; Kepko and Spence, 2003; Claudepierre et al., 2009; Sarris et al., 2010), or as a result of variations in the large-scale convective motion of the magnetosphere driven by changes in the global magnetospheric reconnection rate and the flow of solar wind around the magnetopause (Ridley et al., 1998; Ruohoniemi and Greenwald, 1998).

There are a number of reviews in the literature that discuss proposed modes of interaction between radiation belt particles and Pc-5 ULF waves (e.g. Friedel et al., 2002; Elkington, 2006; Shprits et al., 2008). Large-scale field variations at frequencies commensurate with the particle drift frequency break the drift invariant while maintaining the gyro and bounce invariants associated with trapped particle motion (Roederer, 1970), resulting in a radial drift across field lines and concurrent change in energy. Radial diffusion is a particular case that describes the stochastic motion of an ensemble of particles under the effect of a continuum of ULF waves near the particle drift frequency. Depending on the global particle distribution with respect to the radial coordinate, radial diffusion may act to either increase flux levels in the inner magnetosphere as particles diffuse inward from regions of higher phase space density near the trapping boundary (e.g. Hudson et al., 2012), or, if there is a paucity of electrons at the trapping boundary (e.g. Green et al., 2004; Shprits et al., 2006; Loto'aniu et al., 2010; Turner et al., 2012), act as a loss process as the aggregate particles drift outward and are lost to the magnetopause.

In this diffusive case, the effect of ULF waves on trapped energetic particles may be quantitatively determined by solving the Fokker-Planck equation, including appropriate diffusion coefficients governing the radial transport of particles that results from interaction with global ULF waves. For field variations that break the third adiabatic invariant only (Schulz, 1996), the Fokker-Planck equation reduces to the well-known radial diffusion form,

$$\frac{\partial f}{\partial t} = L^2 \frac{\partial}{\partial L} \left[\frac{D_{LL}}{L^2} \frac{\partial f}{\partial L} \right] - \frac{f}{\tau_I},\tag{4.1}$$

where f is the drift-averaged distribution function or reduced phase space density and τ_L represents the particle lifetime.

Early analytic formulations of the relevant transport coefficients D_{LL} have been given by Fälthammar (1965, 1966a, b, 1968), Cornwall (1968), and Schulz and Lanzerotti (1974), among others. Assuming a time-varying potential (i.e. curl-free) electric field, such as may result from the uniform global convection associated with the Dungey cycle (Dungey, 1961), the form of the radial diffusion coefficient is

$$D_{LL}^{E} = \frac{1}{8B_{E}^{2}R_{E}^{2}}L^{6}\sum_{m}P_{m}^{E}(m\omega_{d}). \tag{4.2}$$

The transport coefficients that result from variations in the magnetic field is given as

$$D_{LL}^{B} = \frac{M^{2}}{8q^{2}\gamma^{2}B_{E}^{2}R_{E}^{4}}L^{4}\sum_{m}m^{2}P_{m}^{B}(m\omega_{d}),$$
(4.3)

(Fei et al., 2006). In these expressions, m is the azimuthal mode number of the ULF waves driving the diffusion, M is the first adiabatic invariant, γ is the Lorentz factor, q is the particle charge, $B_E = 0.31$ Gauss, and R_E is an Earth radius. \mathcal{P}_m^B and \mathcal{P}_m^E are the power spectral densities of the compressional magnetic field and the potential electric field, both evaluated at the resonant wave frequency

$$\omega = m\omega_d, \tag{4.4}$$

where ω_d is the particle drift frequency (Elkington et al., 1999, 2003). It should be noted that this drift-resonant frequency condition specifies the population of particles that will be affected by a given frequency band of ULF waves, since the drift frequency is energy-dependent.

Note that the form (4.3) is relativistically correct and general in terms of the power spectral density, in contrast to the form offered by Fälthammar (1966a, 1968), which was for nonrelativistic particles and assumed a power spectrum that decreased

as ω^2 . Under the assumptions used in Fälthammar, an explicit L^{10} dependence appears in the diffusion coefficient, in contrast to the L^4 dependence exhibited in Equation (4.3).

4.2 Questions: Quantitative determination of transport rates

There have been numerous and ongoing efforts to quantify the radial transport rates suggested in Equations (4.2) and (4.3) based on observations of electric and magnetic field variations. For example, Brautigam et al. (2005) used electric field measurements from the CRRES spacecraft to calculate radial diffusion coefficients based on a functional fit of \mathcal{P}_m^E as a function of radial position, L, and the magnetospheric activity parameter K_p . They found that the diffusion coefficient, D_{LL} , could vary by 1-2 orders of magnitude between low activity $(K_p = 1)$ and high activity $(K_p = 6)$, depending on L and the first (gyro) invariant. However, the nature of the single-point electric field measurements forced them to consider only the diffusive effects of the curl-free part of the electric field variations, to assume only the m = 1 azimuthal resonance, and that the power was uniformly distributed in local time. Rae et al. (2012) used ground magnetometers to examine the local time distribution of ULF wave power in the electric field as a function of solar wind speed, and Ozeke et al. (2012) used a combination of ground- and space-based observations to extend these analyses to magnetic field fluctuations. In this latter work they obtained coefficients using assumed values of m, held constant at all radial distances and frequencies. These results also contrasted with earlier empirical efforts to quantify radial diffusion by Brautigam and Albert (2000), in that the effects of electric field activity at ULF frequencies were determined to be more important than the magnetic field variations in driving particle dynamics.

Key to quantitatively describing the effect of radial transport on radiation belt particles is understanding the global spectral and spatiotemporal characteristics of magnetospheric ULF waves. In the remainder of this chapter we outline the fundamental questions that must be addressed to fully describe the relevant radial diffusion transport coefficients, Equations (4.2) and (4.3), and discuss recent progress in understanding the characteristics of ULF waves and their resulting effects on radiation belt dynamics.

4.2.1 What is the power spectrum as a function of frequency?

There are several explicit and implicit functional dependencies in Equations (4.2) and (4.3). The power spectral density terms $\mathcal{P}_m^{E,B}$ prominently suggest the need for a quantitative measure of the ULF wave activity. In particular, this activity should be

quantified at the drift resonant frequency given by Equation (4.4) for the particle population in question, rather than a frequency-integrated measure of the wave spectrum. Appropriate measures of the power spectral density for use in Equations (4.2) and (4.3) can be obtained in a relatively straightforward fashion using the periodogram spectral density methods described in Press et al. (1992).

The means of measuring the relevant electric and magnetic field fluctuations presents a main challenge in calculating relevant diffusion coefficients. To understand the transport problem throughout the radiation belts, one would ideally have access to the time-dependent field fluctuations at multiple simultaneous locations throughout space. In practice, measurements are limited to what one can infer about ULF fluctuations in space from ground magnetometers (e.g. Mann et al., 2008), and from in situ observations located at only a few points in space. Geosynchronous orbit provides an appropriate platform for simultaneous measurements of magnetic ULF power at a number of local times along a nominal particle drift orbit (e.g. Perraut et al., 1978; Singer et al., 1996; Huang et al., 2010; Clausen et al., 2011; Ozeke et al., 2012). For example, Bloom and Singer (1995) used geosynchronous measurements to examine trends in the power spectral density as a function of frequency, finding generally increasing power with decreasing frequency in the Pc-2 (~0.1 Hz) through Pc-5 (mHz) bands, as indicated in Figure 4.1.

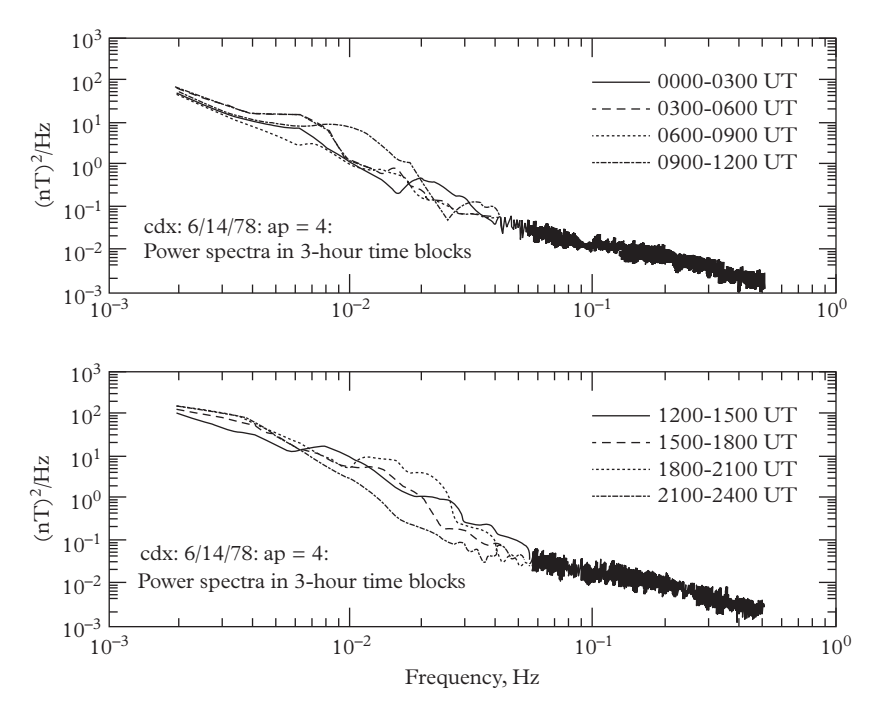


Figure 4.1 Magnetic ULF wave power at geosynchronous orbit as a function of frequency. After Bloom and Singer (1995).

We note that the power spectral density as a function of wave frequency alone is insufficient to determine the resonant frequency at a particular point in space given by Equation (4.4) for a given particle population; one also needs some estimate of the distribution of energy across azimuthal modes, discussed below. However, in low-mode number situations such as are afforded in "breathing mode" magnetic fluctuations driven by solar wind pressure variations, an m = 1 assumption may be sufficient to quantitatively tie the wave frequency to the particle drift frequency (Tu et al., 2012).

4.2.2 What is the radial profile of the ULF activity?

In addition to the explicit radial dependence appearing in each term in Equations (4.2) and (4.3) (i.e. L^4 in the magnetic term, L^6 in the electric term), the power spectral density terms $\mathcal{P}_m^{E,B}$ have an implicit radial dependence. This may be particularly pronounced in regions near Field Line Resonances (FLRs), quasisinusoidal signals with relatively high wave power at confined radial distances. The absence or presence of ULF wave power at radial locations relative to any peaks in the phase space density profile (e.g. Shprits et al., 2006; Turner et al., 2012) of trapped radiation belt electrons determine whether Pc-5 ULF waves will act as an acceleration or loss process in the radiation belts. Thus, it is necessary to understand the radial structure of ULF wave power in the magnetosphere to determine the effect of transport in the radiation belts.

The CRRES (Wygant et al., 1992; Singer et al., 1992), Polar (Russell, 1995), Cluster (Escoubet et al., 1997), and THEMIS (Sibeck and Angelopoulos, 2008) missions are among those that have provided insight into electric and magnetic field power at different L values along their respective orbital tracks (Brautigam et al., 2005; Sarris et al., 2009a; Liu et al., 2009a, 2010; Loto'aniu et al., 2010; Ozeke et al., 2012), providing a global picture of ULF wave power spectral density in local time and L over the course of their respective precession times. An example from Liu et al. (2009b) is indicated in Figure 4.2, which shows magnetic and electric field amplitudes and power spectral densities along a single radial profile traversed by the spacecraft THEMIS-D from the nominal plasmapause position at \sim 4.5 R_E to the magnetopause at \sim 9.5 R_E . Although there are particular peaks in the power spectral density corresponding to the coherent FLR activity evident in the field amplitude panels, the general trend is for higher power at lower frequency, consistent with the geosynchronous observations suggested in Figure 4.1. Another noticeable feature is for the peak power spectral density to trend to lower frequencies as the spacecraft traverses to higher L values, reflecting that the resonant frequency for a given field line (at constant density) decreases as the Alfvén speed decreases with decreasing B, and also decreases as the total field line length increases (Kivelson and Southwood, 1988). Finally, the power increases somewhat with increasing radial distance, an effect most clearly pronounced in the radial and compressional magnetic field components at L values approaching the magnetopause.

Ionospheric conductivity effects will tend to modify the polarization and amplitude of ULF wave activity observed on the ground (Hughes, 1974), but not the frequency spectrum of the fluctuations. This allows a relative measure of space-based magnetic

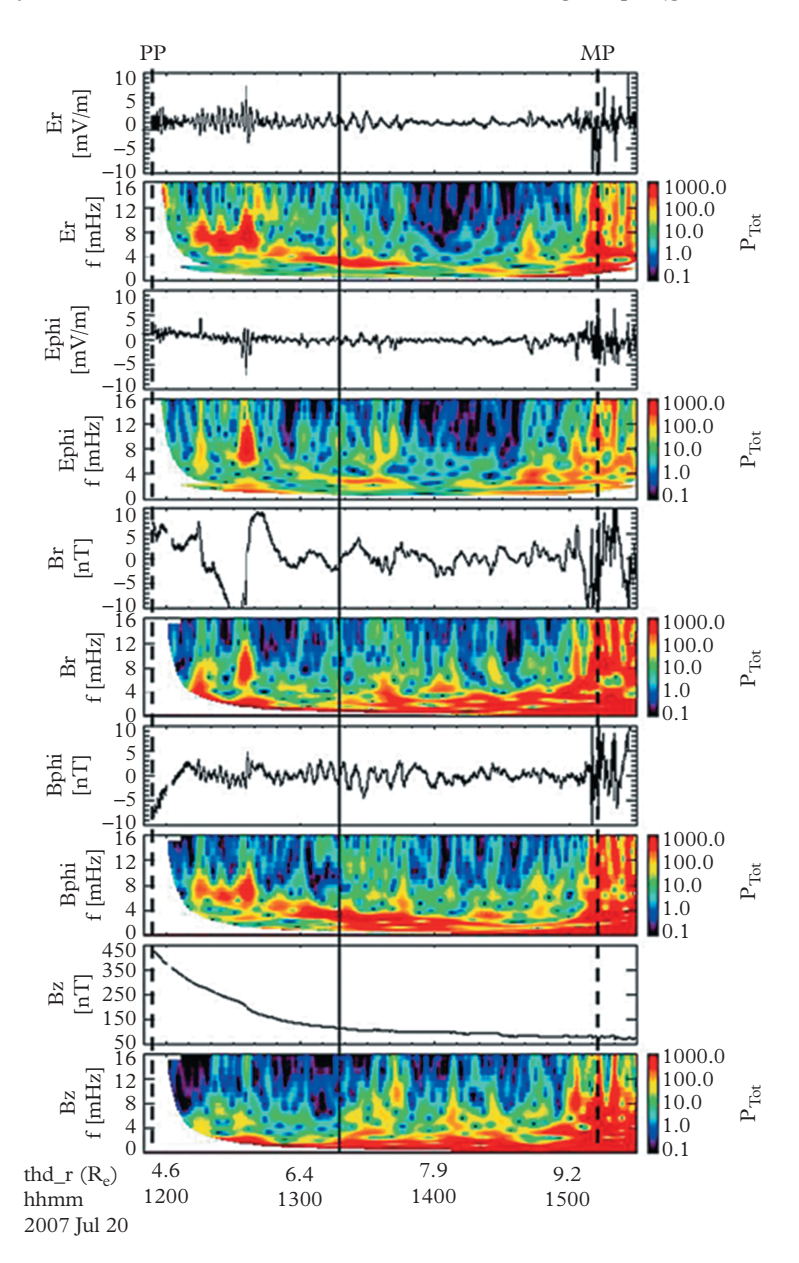


Figure 4.2 Magnetic and electric ULF wave power along a radial cut from the THEMIS-D spacecraft (Liu et al., 2009b).

field variations over a wide range of latitudes and local times, but does not provide absolute amplitude of the associated compressional magnetic field components in space required in Equation (4.3). However, the work of Ozeke et al. (2009) provides a means of mapping magnetometer fluctuations corresponding to guided poloidal and toroidal mode Alfvénic electric fluctuations (Kivelson and Southwood, 1988). This technique allows simultaneous observation of the equatorial electric field fluctuations over a distribution of local times and radial distances in space. Rae et al. (2012) and Ozeke et al. (2012) have used this technique to investigate the global dependence of ULF electric wave power on local time, radial distance, and geomagnetic activity based on magnetometer observations from the CARISMA magnetometer array. An example is indicated in Figure 4.3, which for moderate driving conditions again indicates the features discussed above; namely, decreasing power with increasing frequency and increasing power with increasing radial distance.

4.2.3 What is the azimuthal mode structure?

Explicit in the radial transport rates given by Equations (4.2) and (4.3) is the dependence on the azimuthal mode structure of a given population of waves, characterized by the mode number m. This dependence dictates which particles will be effectively transported in the interaction, based on the variation of drift velocity with particle energy and the drift resonance condition $\omega - m\omega_d = 0$. Figure 4.4 provides a simple, idealized sketch showing how the mode structure may be interpreted for the m=1 and m=2 global ULF modes, where the phase here provides symmetry about the Earth–Sun line. Here the shaded regions represent either a positive or negative field perturbation, while the unshaded regions show field perturbations of the opposite sign. The line of transition between the shaded and unshaded region represent nodes between the perturbed regions. The azimuthal mode number, m, is a measure of the wavelength, and is calculated based on the number of azimuthal wavelengths that would fit within a particle drift orbit.

In the simplest application, unambiguously determining the azimuthal mode structure to a particular mode number m requires 2m uniform azimuthal measurements. Because an appropriate azimuthal distribution of in situ measurements is rare in the magnetosphere, it is common to make an explicit or implicit assumption about the mode distribution of the ULF wave power. For example, it is often implicitly or explicitly assumed that all power is in the m=1 mode of the waves being measured (e.g. Shprits and Thorne, 2004; Shprits et al., 2009; Brautigam et al., 2005). By contrast, Hudson et al. (1999, 2001) and Loto'aniu et al. (2006) explicitly assumed an m=2 mode spectrum.

While most studies by necessity assume a single mode number, notable exceptions may be found in the work by Fei et al. (2006), Tu et al. (2012) and Elkington et al. (2012), who used mode spectrum results obtained from a Lyon-Fedder-Mobarry (LFM) MHD simulation (Lyon et al., 2004) to calculate the ULF wave azimuthal mode numbers. They found that, even though the magnetic power calculated at m=1 in the MHD simulations was dominant for some parts of the events they studied, at times,

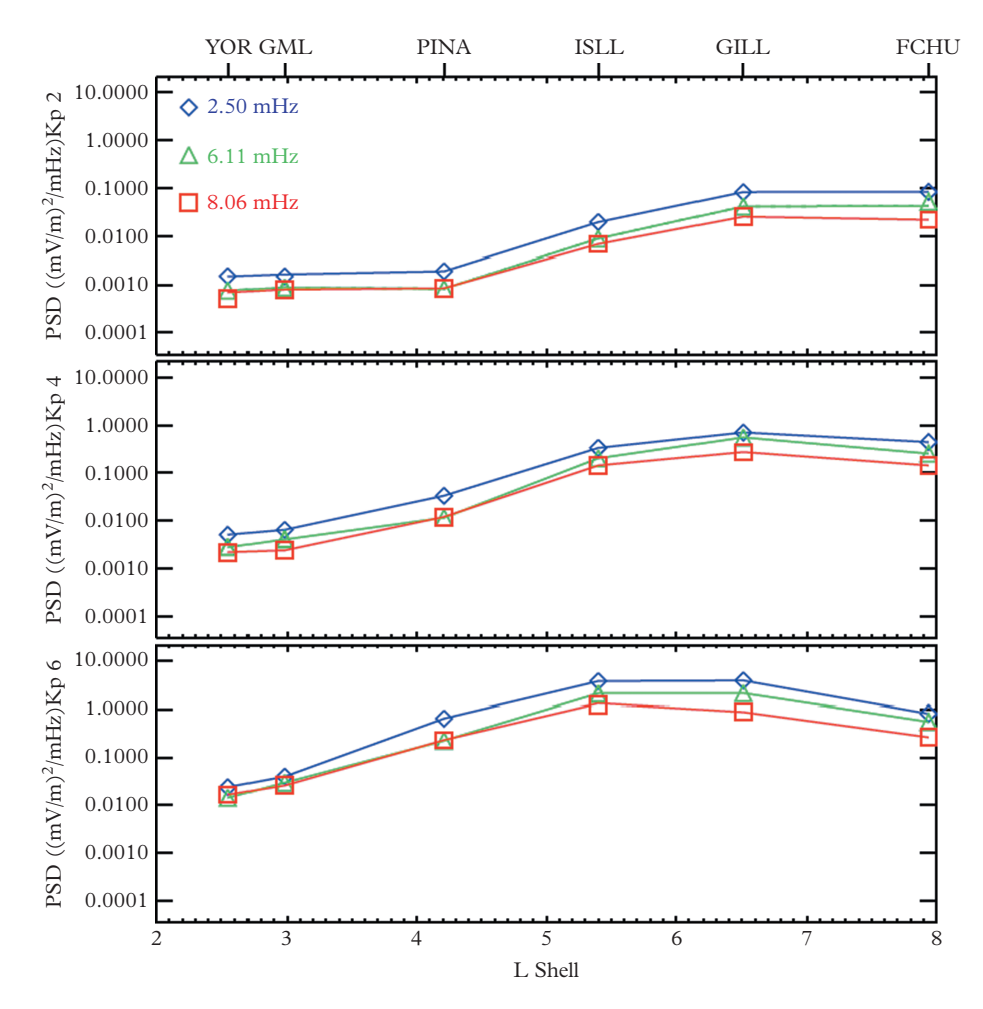


Figure 4.3 Electric ULF wave power in the equatorial plane, derived from magnetic fluctuations observed at a number of latitudinally-distributed ground magnetometers (Ozeke et al., 2012).

assuming that all power comes from m=1 may may lead to overestimation of the power capable of drift-resonantly interacting with a given particle population via the $\omega=\omega_d$ resonance, and underestimating the transport of higher-energy particles that may interact with m>1 resonances. This was particularly true during the main phase of a geomagnetic storm. These studies also found that, overall, assuming that the total B_z power from the m=1 mode (related to the solar wind dynamic pressure variations) is a reasonable approximation, while the electric field had substantial m>1 power, which is mostly related to night-side geomagnetic activity associated with substorm-induced flow channels and global magnetospheric convective patterns.

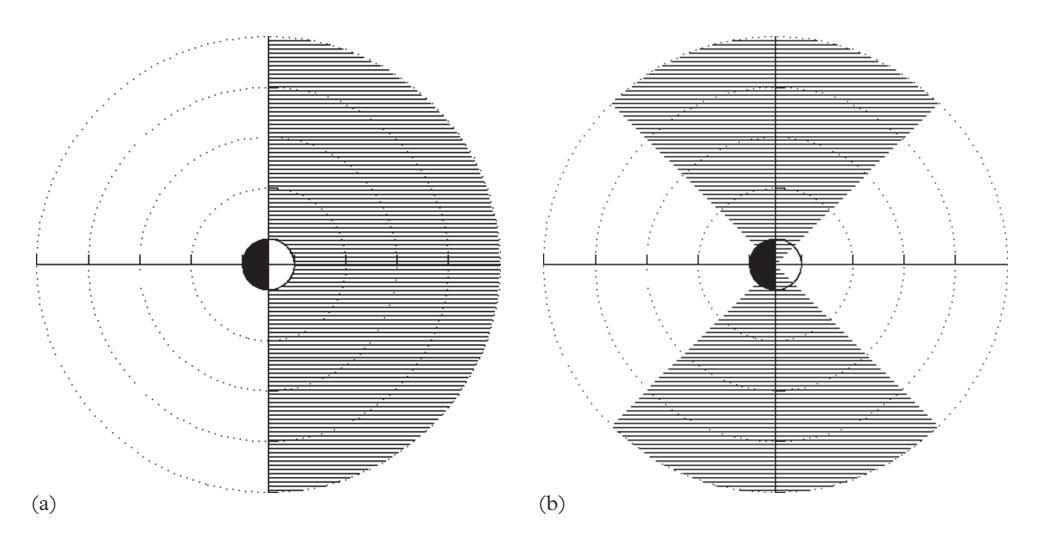


Figure 4.4 Simple interpretation of the nodal structure of the m = 1 and m = 2 modes of global ULF wave activity at an instant of time. In this figure the shaded regions represent regions of positive or negative field perturbation, while the unshaded regions represent local times with oppositely-signed perturbation. The line of transition between the shaded and unshaded region represent nodes between the perturbed regions.

Figure 4.5 shows the fraction of the total power spectral density in each mode, for the equatorial azimuthal electric field and magnetic field for the September 24–26, 1998 geomagnetic storm studied by Elkington et al. (2012). The integrated power represents the power spectral density summed over all mode numbers representable on the azimuthal MHD grid, $\sum_{m=0}^{24} P_m$, integrated in frequency up to the temporal Nyquist frequency. The fractional power in each mode for the m=1, 2, and 3 modes are indicated in the lower of each pair of plots by the solid, dotted, and dashed lines, respectively, and the fractional power of the sum of the first five modes plotted using "+" symbols.

We see in Figure 4.5 that the m=1 mode is generally dominant in both the electric and magnetic fields during the recovery phase, with much smaller contributions from the m=2 and 3 modes. However, during the main phase the electric field power exhibits relatively large contributions from the m=2 and 3 modes; for a period of time the power in these modes is actually larger than the power in the m=1 mode. In this event we see much more structure in the electric field than the magnetic field during the main phase, with the power in the first three mode numbers accounting for only $\sim 60\%$ of the total power, in contrast to closer to $\sim 80\%$ in the case of the magnetic power. During the recovery phase the power is concentrated in the lower mode numbers for both the electric and magnetic fields, with the lowest three mode structures accounting for $\sim 80\%$ of the power in both cases. These results are consistent in the simulations both at geosynchronous altitudes and at equatorial radial distances of 4.2 R_E , corresponding to altitudes of the GPS constellation of spacecraft.

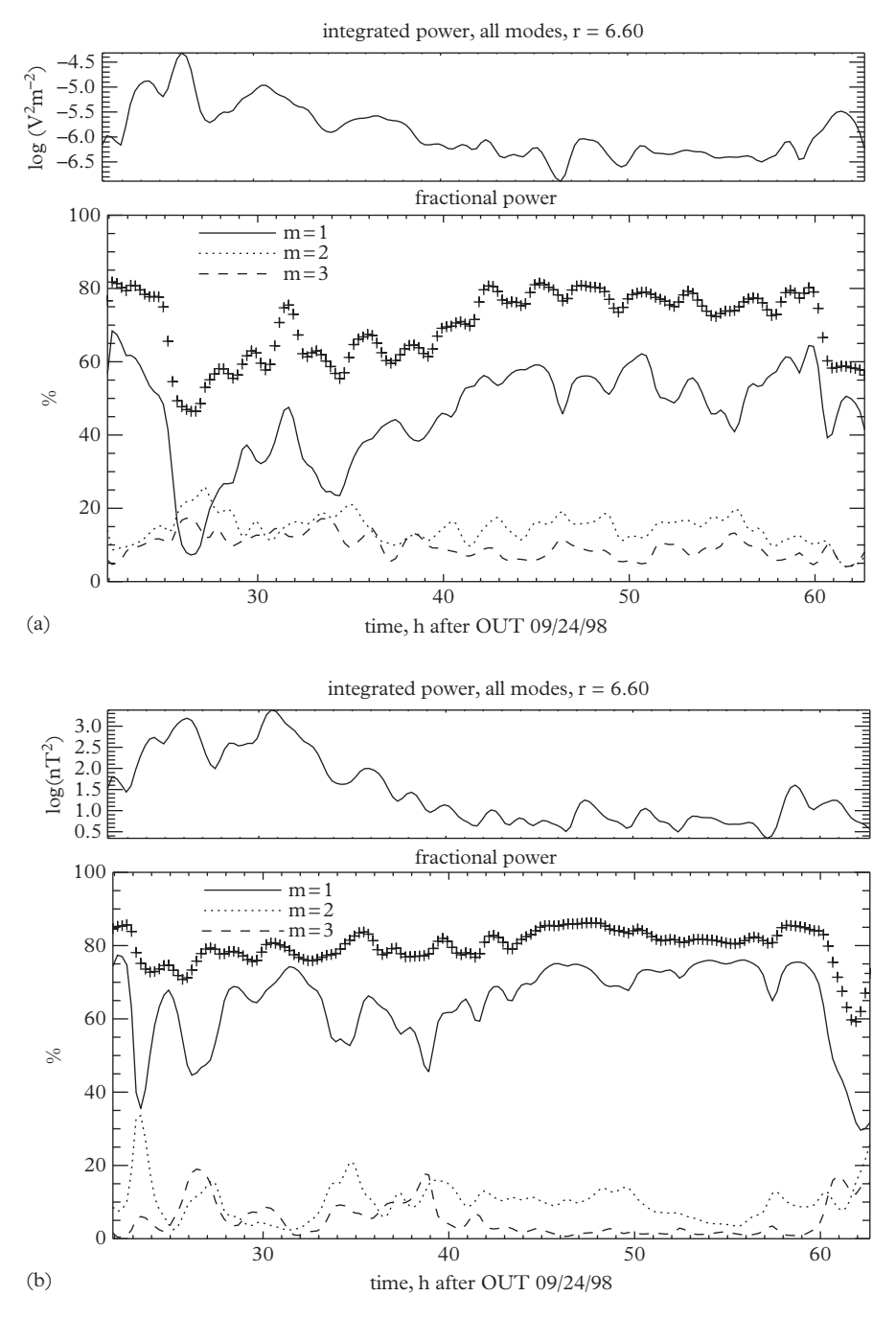


Figure 4.5 Fraction of the power in the lowest three mode numbers for the electric (a) and magnetic (b) ULF wave fields. In the top of each pair of plots we indicate the total power spectral density over all azimuthal modes as a function of time. The '+' symbols in the bottom of each pair of plots indicates the fraction of power in the sum of the first 5 modes as a fraction of the total power; the remaining lines indicate the power in each of the first three modes. (Elkington et al., 2012).

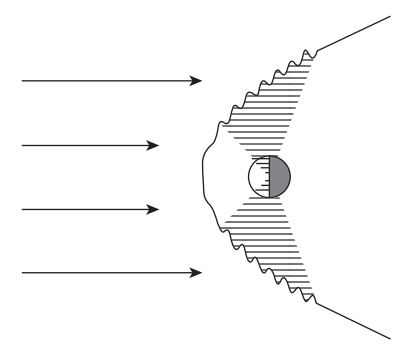


Figure 4.6 Sketch of Kelvin-Helmholz waves generated by sheer interactions along the flank magnetopause, illustrating the difference between azimuthal extent (indicated by the shaded regions) and azimuthal wave number (indicated by the recurring wavelengths along the magnetopause).

4.2.4 What is the azimuthal extent?

Distinct from the azimuthal mode structure of the waves is the azimuthal extent of the wave power. This distinction is illustrated in Figure 4.6, which shows a schematic of shear-driven ULF waves on the flanks. The azimuthal extent of the waves is indicated by the shaded region and extends over several hours of local time on the dawn and dusk flanks. The mode number, by contrast, is indicated by the wavelength, λ , of the waves, with several cycles occurring over the region where the shear waves are induced. Quantitatively, $m \equiv 2\pi/\lambda$. Simulations of magnetopause Kelvin-Helmholz waves undertaken by Claudepierre et al. (2008) suggest that typical mode numbers of these waves lie in the range m = 12-15, corresponding to 1–2 h of local time, while the azimuthal region where the waves occur typically subtends several hours of local time.

Geosynchronous observations of magnetic Pc-5 fluctuations via the NOAA GOES spacecraft have provided continual, long-term measurements of magnetic ULF wave power, covering all local times once per day. Huang et al. (2010) conducted a statistical study of ULF wave power in all three components of the magnetic vector perturbations as a function of frequency, local time, solar wind driving, and geomagnetic activity. They found a preponderance of power in the compressional magnetic field on the dayside resulting from pressure fluctuations that increased with increasing solar wind velocity, and additional regions of power in the midnight sector probably associated with substorm activity. Tu et al. (2012) studied a particular magnetic storm associated with high speed solar wind regions, and similarly found peaks in the compressional component of magnetic ULF wave activity in the noon sector extending through dusk. Clausen et al. (2011) studied 17 storms associated with variable radiation belt electron populations, and also found that most power in the frequency ranges associated with particle drift frequencies occurred in the compressional mode in the noon sector.

Liu et al. (2009b) examined THEMIS magnetic field data to derive a statistical model of Pc-5 ULF wave power in FLRs at all local times for a range of *L* shells. In contrast to the earlier work of Anderson et al. (1990), who used AMPTE/CCE data to find that shear Pc-5 waves were more frequently seen on the dawnside magnetosphere, Liu et al. suggested that compressional field line resonances were more prevalent on the duskside but that shear-mode Pc-5 waves were evenly distributed in azimuth.

The azimuthal distribution of Alfvénic electric field variations were obtained from ground magnetometers by Rae et al. (2012) using the mapping techniques described in Ozeke et al. (2009). Figure 4.7 indicates the results obtained for the GILL magnetometer, magnetically mapping to a point near geosynchronous orbit. Consistent with the in situ geosynchronous observations of magnetic field fluctuations, they found increasing power at all local times with increasing solar wind speed. Consistent with the Anderson et al. (1990) results, they found significantly more power on the dawnside in the shear mode (associated with radial electric fields) and in ground measurements associated with azimuthal electric fields. Notable in Figure 4.7 are the peaks in power spectral density in the 3–5 mHz range in the noon, dawn, and dusk sectors, likely associated with driven FLR activity. Aside from the peak in power associated with FLRs seen at noon, differences in the power spectral densities seen at noon and midnight were roughly of the same order of magnitude.

4.2.5 What is the propagation direction?

The wave frequency ω in Equation (4.4) may take on either positive or negative values, signifying the direction of phase propagation of the ULF waves. Understanding the propagation direction is key in assigning wave power appropriately to particle populations, as the drift-resonant nature of the interaction underlying transport expressions (4.2) and (4.3) requires that a particle drift with a phase speed commensurate with the phase propagation speed of the wave. That is, the particle should see a field with a relatively constant sign associated with the wave as the particle and wavefront move together in azimuth. For trapped electrons, drifting in a right-hand sense about the Earth, the wave frequency (4.4) should be positive; for protons, with their oppositely-directed drift sense, the frequency should be negative.

Mann et al. (1999) discussed the excitation of magnetospheric waveguide modes, whereby wave energy was converted from plasma flows in the magnetosheath to enhanced ULF wave energy propagating tailward through the magnetosphere. For protons drifting in a counter-clockwise sense about the Earth, most of the ULF-related acceleration under this scenario would occur in the dawn sector. Conversely, electrons would experience most of their acceleration from this tailward propagation of energy in the dusk sector.

Properly assigning a propagation direction to a given wave observation may be difficult. For waves originating from a known source, such as for shear waves propagating tailward along the flanks of the magnetopause, assigning propagation direction may be intuitively clear. This assumption is obviously complicated in situations where E and B fluctuations may be arising from multiple sources, such as in the dawn-midnight or dusk-midnight sectors, where one may reasonably expect to see tailward-propagating waves resulting from solar wind pressure perturbations at the magnetopause or Kelvin-Helmholz waves generated at the flanks, mixed with sunward-propagating waves resulting from substorm activity or global convection. Descriptions of the Poynting vector hold promise as a means of examining wave propagation direction, but can

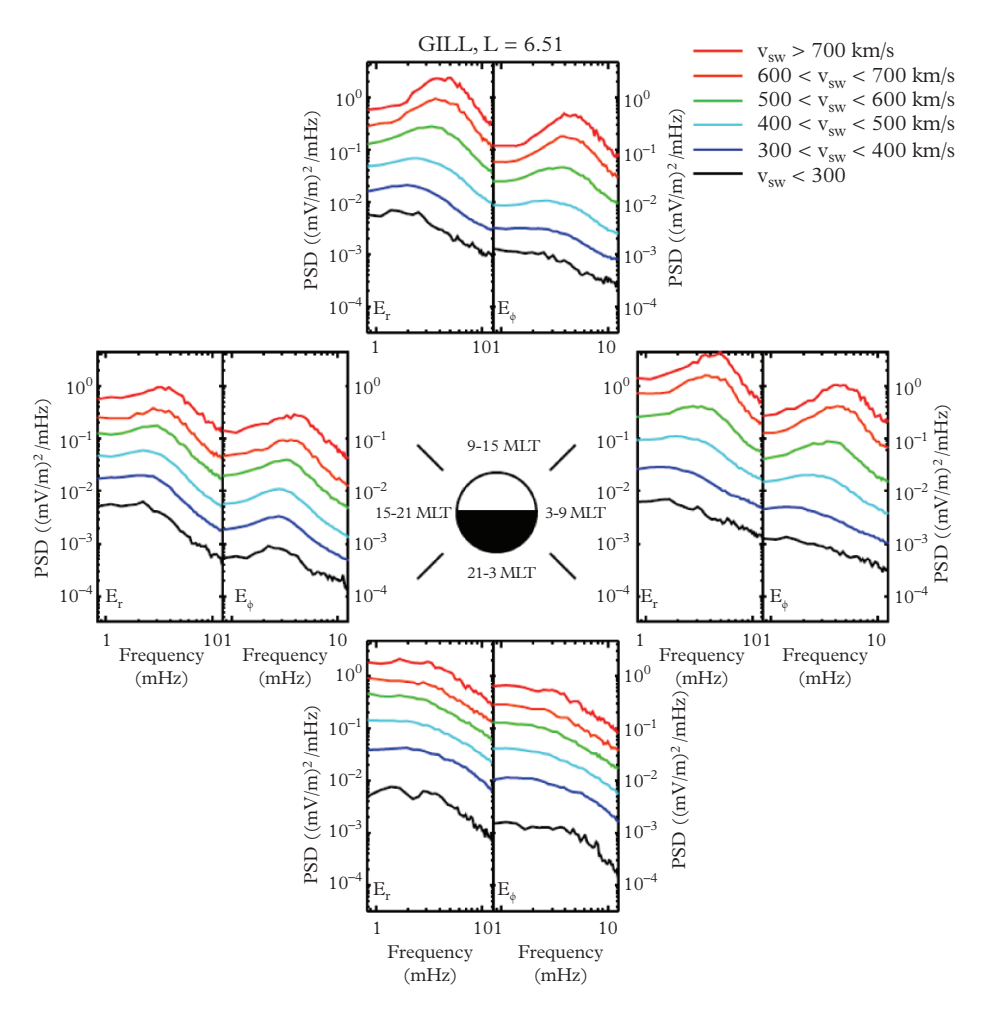


Figure 4.7 Electric ULF wave power near geosynchronous as a function of solar wind velocity and local time, for toroidal shear (E_{ϕ}) and poloidal (E_r) ULF wave modes (Rae et al., 2012).

be similarly complicated at points in space where a superposition of wave activity arising from multiple sources is present.

Figure 4.8 shows initial work to quantify ULF energy propagation in the inner magnetosphere via calculation of a mean Poynting vector at different locations in the magnetosphere (Hartinger et al., 2013). This study found significant scatter in Poynting vector direction at all locations and frequencies studied. However, for Pc-5 waves propagating with an azimuthal component likely to transport energetic particles trapped in the inner magnetosphere, there was a preference for duskward and earthward energy transfer on the dayside, and a preference for sunward Poynting vectors in the predawn

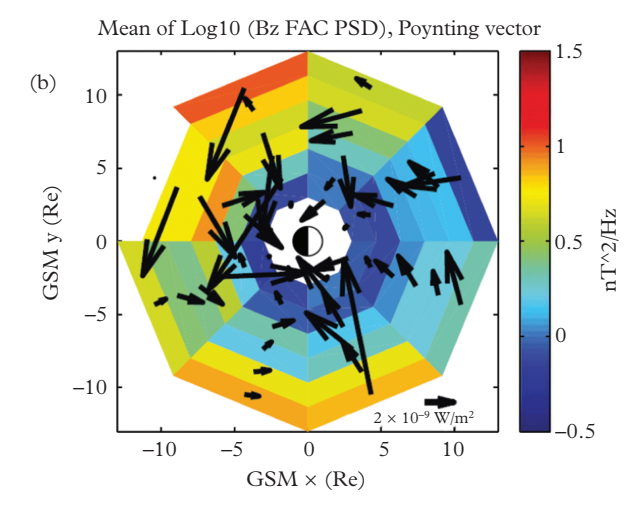


Figure 4.8 6mHz parallel magnetic power spectral density on the color scale, along with of the GSM projection of the mean Poynting vector. Via Hartinger et al., (2013)

sector potentially associated with substorm activity. Both of these situations would tend to transport/accelerate trapped energetic electrons.

4.2.6 What is the origin of the waves?

Finally, one needs to assign an electrostatic or electromagnetic character to the waves in order to properly quantify the transport rates via Equations (4.2) or (4.3), respectively. This is difficult under circumstances of a single point in-situ measurement, as electromagnetic waves will have non-zero curl in the electric field and will require additional assumptions regarding spatial structure to properly resolve the global field character. For example, potential waves resulting from variations in the convection electric field were envisioned in the formulation of Equation (4.2) in the original derivation by Fälthammar (1965). However, in the same paper Fälthammar includes the effect of electric fields induced by magnetic field variations in the equation analogous to Equation (4.3). In this formulation, magnetic field fluctuations were responsible for 7/15 of the resulting radial diffusion, while the electric field fluctuations induced by the magnetic field were responsible for the remainder of the transport term.

A single-point measurement of E and B cannot disambiguate how much of the electric field power is appropriate to assign to Equation (4.2) and how much of the electric field power is implicit in Equation (4.3), leading to the potential for "overcounting" the effect of measured electric fields. Some work, for example Fei et al. (2006), assumed that the electric and magnetic field fluctuations were completely decoupled, and assigned all electric field power to Equation (4.2) assuming magnetic field fluctuations were the only term contributing to Equation (4.3). However, this is an imperfect approach due to the clear phase relationships between the driven magnetic variations and the corresponding induced electric field variations (Perry et al., 2005).

According to the Helmholz theorem, a vector may be completely specified in terms of its divergence, curl, and a normal component described over a boundary (e.g. Arfken, 1985). Assuming charge neutrality, the problem in space physics is reduced to that of measuring a curl and specifying appropriate boundary conditions. Constellations of at least four spacecraft, such as are available via the Cluster mission (Escoubet et al., 1997), are capable of uniquely determining the curl of the electric field on spatial scales appropriate to the spacecraft separation. However, determination of an appropriate boundary condition among the dynamic E and B fields in the near-Earth space environment, allowing specification of the curl of the electric field at all spatial scales, remains a significant challenge in sorting out this problem.

4.3 Conclusions and future possibilities

Complete specification of the effects of Pc-5 ULF wave-driven transport requires global knowledge of the character of ULF waves, quantified by the questions outlined in this chapter. Previous in situ observations, both at geosynchronous and across L shells, have provided statistical characterizations of the spatial (i.e. radial and azimuthal) and spectral characteristics of wave activity under different driving conditions. These quantities have been incorporated into empirical models of radial diffusion coefficients, for example, provided by Brautigam and Albert (2000) or Ozeke et al. (2012). The quality of these empirical diffusion coefficient models can be traced back to the comprehensiveness of the data that was used to build them, and are not always consistent with each other (for example, Brautigam and Albert (2000) suggests a dominant role for magnetic diffusion, Equation (4.3), while Ozeke et al. (2012) suggests a larger role for electric diffusion, Equation (4.2)). However, these empirical specifications have been used with some success in driving dynamic models of the radiation belts (e.g. Shprits et al., 2005; Lam et al., 2007; Tu et al., 2013). The recent launch of the Van Allen Probe mission (Mauk et al., 2013), consisting of a pair of identically-instrumented spacecraft in a "string of pearls" geotransfer orbit, promises to do much to increase our understanding of the occurrence and characteristics of the low frequency waves that lead to transport through Equation (4.1).

Quantifying dynamic changes in the radiation belts via application of the diffusion Equation, (4.1), requires not only careful quantification of the diffusion coefficients, but also of the spatial characteristics of the distribution function, f. This is evidenced by the dependence of Equation (4.1) on the radial gradient of the phase space density on the right-hand side of Equation (4.1). Here again the Van Allen Probes hold promise to improve our understanding of the spatial evolution of the distribution function, including quiescent configurations that may be used as initial conditions in dynamic models of the radiation belts.

Remaining questions necessary to quantify the ULF-driven transport of radiation belts in terms of the transport coefficients (4.2) and (4.3) include better understanding of the mode structure, propagation direction of ULF waves, and the

electromagnetic character of waves arising from different sources. As mentioned in Section 4.3, unambiguously determining the mode structure to mode number m requires 2m measurements. As it is unlikely that the number of in-situ measurements required to evaluate any more than the lowest-order mode structure will be achieved in the near future, alternative methods are being developed. For example, cross-wavelet analysis between time series is used increasingly in geophysical data analysis in order to examine if regions in time and frequency with large common power also have a consistent phase relationship (e.g. Grinsted et al., 2004; Sarris et al., 2009b, 2012). These methods may be used to infer or constrain the global mode structure based on a few azimuthally-separated measurements. In the case of magnetospheric electric variations, these techniques will be augmented through the mapping techniques suggested by Ozeke et al. (2009). Additional information about the mode structure may be obtained by combining global MHD models of the magnetospheric system (Tu et al., 2012; Elkington et al., 2012) with these new measurements.

Determining the propagation direction and electromagnetic character of measured waves remain significant challenges. Poynting vector calculations (Hartinger et al., 2013) hold some promise in evaluating propagation direction, but can be confounded in regions where waves from multiple sources may be propagating in different directions through the magnetosphere. Presumably better estimates of propagation direction will be obtained as we improve understanding of the various global drivers and dynamics of the magnetospheric system. Determining the electromagnetic character of the waves also presents a challenge. Again, this may be relatively easy to do in cases where clear phase relations between measured E and B variations are available, such as in the case of strong FLR activity. In the more general case, separating the curl-free component of the electric field from the total electric field requires knowledge of the spatial distribution of the fields around the point in question. Constellation missions such as provided by Cluster, perhaps combined with global physical simulations of the geospace environment, may hold promise in disentangling the appropriate partitioning of measured electric fields between the potential and induced electric fields explicit in Equation (4.2) and implicit in Equation (4.3).

Acknowledgments

Work has been supported by NSF grant ATM0842388 and NASA grants NNX09AI05G, NNX10AQ50G, NNX13AE39G, NNX10AQ48G and NNX14-AC04G at the University of Colorado/LASP. Additional support provided by the European Union (European Social Fund—ESF) "Investing in Knowledge" and Greek national funds through the Operational Program "Education and Lifelong Learning" of the National Strategic Reference Framwork (NSRF) Research Funding Program: Thales. The authors thank I.R. Mann, D.K. Milling and the rest of the CARISMA team for data. CARISMA is operated by the University of Alberta, funded by the Canadian Space Agency.

.....

REFERENCES

- Anderson, B. J., M. J. Engebretson, S. P. Rounds, L. J. Zanetti, and T. A. Potemra (1990), A statistical study of pulsations observed by the AMPTE/CCE magnetic fields experiment—1. Occurrence distributions, *J. Geophys. Res.*, **95**, 10,495.
- Arfken, G. (1985), Mathematical Methods for Physicists, 985 pp., Academic Press, Boston.
- Baker, D. N., et al. (1998), A strong CME-related magnetic cloud interaction with the Earth's magnetosphere: ISTP observations of rapid relativistic electron acceleration on May 15, 1997, *Geophys. Res. Lett.*, 25, 2975.
- Bloom, R. M., and H. J. Singer (1995), Diurnal trends in geomagnetic noise power in the Pc2 through Pc5 bands at low geomagnetic latitude, *J. Geophys. Res.*, 100, 14,943.
- Brautigam, D. H., and J. M. Albert (2000), Radial diffusion analysis of outer radiation belt electrons during the October 9, 1990, magnetic storm, J. Geophys. Res., 105(A1), 291.
- Brautigam, D. H., G. P. Ginet, J. M. Albert, J. R. Wygant, D. E. Rowland, A. Ling, and J. Bass (2005), CRRES electric field power spectra and radial diffusion coefficients, J. Geophys. Res., 110(A2), A02,214, doi:10.1029/2004JA010612.
- Cahill, L. J., Jr., and J. R. Winckler (1992), Periodic magnetopause oscillations observed with the GOES satellites on March 24, 1991, J. Geophys. Res., 97(A6), 8239.
- Chen, L., and A. Hasegawa (1991), Kinetic theory of geomagnetic pulsations 1: Internal excitations by energetic particles, *J. Geophys. Res.*, **96**(A2), 1503–1512.
- Claudepierre, S. G., S. R. Elkington, and M. Wiltberger (2008), Solar wind driving of magnetospheric ULF waves: Pulsations driven by velocity shear at the magnetopause, *J. Geophys. Res.*, 113, A05218, doi:10.1029/2007JA012890.
- Claudepierre, S. G., M. Wiltberger, S. R. Elkington, and M. K. Hudson (2009), Magnetospheric cavity modes driven by solar wind dynamic pressure fluctuations, *Geophys. Res. Lett.*, 36, L13101, doi:10.1029/2009GL039045.
- Clausen, L. B. N., J. B. H. Baker, J. M. Ruohoniemi, and H. J. Singer (2011), ULF wave characteristics at geosynchronous orbit during the recovery phase of geomagnetic storms associated with strong electron acceleration, *J. Geophys. Res.*, 116(A9), A09203, doi:10.1029/2011JA016666.
- Cornwall, J. M. (1968), Diffusion processes influenced by conjugate-point wave phenomena, Radio Sci., 3(7), 740.
- Dungey, J. W. (1961), Interplanetary magnetic field and the auroral zones, *Phys. Rev. Lett.*, 6, 47. Elkington, S. R. (2006), A review of ULF interactions with radiation belt electrons, in *Magnetospheric ULF waves: Synthesis and new directions*, vol. 169, edited by K. Takahashi, P. J. Chi, R. E. Denton, and R. L. Lysak, p. 177, AGU, Washington, D.C.
- Elkington, S. R., M. K. Hudson, and A. A. Chan (1999), Acceleration of relativistic electrons via drift-resonant interaction with toroidal-mode Pc-5 ULF oscillations, *Geophys. Res. Lett.*, **26**(21), 3273.
- Elkington, S. R., M. K. Hudson, and A. A. Chan (2003), Resonant acceleration and diffusion of outer zone electrons in an asymmetric geomagnetic field, *J. Geophys. Res.*, **108**(A3), 1116, doi:10.1029/2001JA009202.
- Elkington, S. R., A. A. Chan, and M. Wiltberger (2012), Global structure of ULF waves during the 2426 September 1998 geomagnetic storm, in *Dynamics of the Earths radiation belts and inner magnetosphere*, vol. 199, edited by D. Summers, I. R. Mann, D. N. Baker, and M. Schulz, p. 127, AGU, Washington, D.C.

- Escoubet, C. P., C. T. Russell, and R. Schmidt (Eds.) (1997), *The Cluster and Pheonix Missions*, Kluwer Academic, Boston, (reprinted from *Space Sci. Rev.*, **79**, nos 1–2, 1997).
- Fälthammar, C.-G. (1965), Effects of time-dependent electric fields on geomagnetically trapped radiation, J. Geophys. Res., 70(11), 2503.
- Fälthammar, C.-G. (1966a), On the transport of trapped particles in the outer magnetosphere, *J. Geophys. Res.*, 71(5), 1487.
- Fälthammar, C.-G. (1966b), Coefficients of diffusion in the outer radiation belts, in *Radiation trapped in the Earth's magnetic field*, edited by B. M. McCormac, p. 398, NATO Advanced Study Institute, Reinhold Book Corp., New York.
- Fälthammar, C.-G. (1968), Radial diffusion by violation of the third adiabatic invariant, in *Earth's particles and fields*, edited by B. M. McCormac, p. 157, NATO Advanced Study Institute, Reinhold Book Corp., New York.
- Fei, Y., A. A. Chan, S. R. Elkington, and M. J. Wiltberger (2006), Radial diffusion simulation of relativistic electron transport by ULF waves in the September 1998 storm, *J. Geophys. Res.*, 111, A12,209, doi:10.1029/2005JA011211.
- Friedel, R. H. W., G. D. Reeves, and T. Obara (2002), Relativistic electron dynamics in the inner magnetosphere a review, *J. Atmos. Solar Terr. Phys.*, **64**(2), 265.
- Green, J. C., T. G. Onsager, T. P. O'Brien, and D. N. Baker (2004), Testing loss mechanisms capable of rapidly depleting relativistic electron flux in the Earth's outer radiation belt, *J. Geophys. Res.*, 109(A12), A12211, doi:10.1029/2004JA010579.
- Grinsted, A., J. C. Moore, and S. Jevrejeva (2004), Application of the cross wavelet transform and wavelet coherence to geophysical time series, *Nonlin. Process Geophys.*, 11, 51.
- Hartinger, M. D., M. B. Moldwin, K. Takahashi, J. W. Bonnell, and V. Angelopoulos (2013), Survey of the UFL wave Poynting vector near the Earth's magnetic equatorial plane, J. Geophys. Res., 118, 6212, doi:10.1002/jgra.50591.
- Hasegawa, A. (1969), Drift mirror instability in the magnetosphere, Phys. Fluids, 12(12), 2642.
- Huang, C.-L., H. E. Spence, H. J. Singer, and W. J. Hughes (2010), Modeling radiation belt radial diffusion in ULF wave fields: 1. Quantifying ULF wave power at geosynchronous orbit in observations and in global MHD model, J. Geophys. Res., 115, A06215, doi:10.1029/2009JA014917.
- Hudson, M. K., S. R. Elkington, J. G. Lyon, C. C. Goodrich, and T. J. Rosenberg (1999), Simulation of radiation belt dynamics driven by solar wind variations, in *Sun-Earth Plasma Connections*, vol. 109, edited by J. L. Burch, R. L. Carovillano, and S. K. Antiochos, p. 171, AGU, Washington, D.C.
- Hudson, M. K., S. R. Elkington, J. G. Lyon, M. J. Wiltberger, and M. Lessard (2001), Radiation belt electron acceleration by ULF wave drift resonance: Simulation of 1997 and 1998 storms, in *Space Weather*, vol. 125, edited by P. Song, H. J. Singer, and G. L. Siscoe, p. 289, AGU, Washington, D. C.
- Hudson, M. K., T. Brito, S. R. Elkington, B. T. Kress, Z. Li, and M. Wiltberger (2012), Radiation belt 2D and 3D simulations for CIR-driven storms during Carrington Rotation 2068, *J. Atmos. Solar Terr. Phys.*, 83, 51, doi:10.1016/j.jastp.2012.03.017.
- Hughes, W. J. (1974), The effect of the atmosphere and ionosphere on long-period magnetospheric micropulsations, *Planet. Space Sci.*, 22, 1157.
- Jacobs, J. A., Y. Kato, S. Matsushita, and V. A. Troitskaya (1964), Classification of geomagnetic micropulsations, J. Geophys. Res., 69, 180.
- Kepko, L., and H. E. Spence (2003), Observations of discrete, global magnetospheric oscillations directly driven by solar wind density variations, *J. Geophys. Res.*, 108(A6), 21–1, doi:10.1029/2002JA009676.

- Kivelson, M. G., and Z.-Y. Pu (1984), The Kelvin-Helmholtz instability on the magnetopause, *Planet. Space Sci.*, 32(11), 1335.
- Kivelson, M. G., and D. J. Southwood (1988), Hydromagnetic waves in the ionosphere, Geophys. Res. Lett., 15, 1271.
- Lam, M. M., R. B. Horne, N. P. Meridith, and S. A. Glauert (2007), Modeling the effects of radial diffusion and plasmaspheric hiss on outer radiatio belt electrons, *Geophys. Res. Lett.*, 34(20), L20112, doi:10.1029/2007GL031598.
- Liu, W., T. E. Sarris, X. Li, S. Elkington, R. Ergun, V. Angelopoulos, J. Bonnell, and K. H. Glassmeier (2009a), Electric and magnetic field observations of Pc4 and Pc5 pulsations in the inner magnetosphere: A statistical study, J. Geophys. Res., 114, A12206, doi:10.1029/2009JA014243.
- Liu, W., et al. (2009b), Observation and modeling of the injection observed by THEMIS and LANL satellites during the 23 march 2007 substorm event, J. Geophys. Res., 114(A00C18), doi:10.1029/2008JA013498.
- Liu, W., T. E. Sarris, X. Li, R. Ergun, V. Angelopoulos, J. Bonnell, and K. H. Glassmeier (2010), Solar wind influence on Pc4 and Pc5 ULF wave activity in the inner magnetosphere, J. Geophys. Res., 115, A12201, doi:10.1029/2010JA015299.
- Loto'aniu, T. M., I. R. Mann, L. G. Ozeke, A. A. Chan, Z. C. Dent, and D. K. Milling (2006), Radial diffusion of relativistic electrons into the radiation belt slot region during the 2003 Halloween geomagnetic storms, *J. Geophys. Res.*, 111(A4), A04218, doi:10.1029/2005JA011355.
- Loto'aniu, T. P., H. J. Singer, C. L. Waters, V. Angelopoulos, I. R. Mann, S. R. Elkington, and J. W. Bonnell (2010), Relativistic electron loss due to ultralow frequency waves and enhanced outward radial diffusion, *J. Geophys. Res.*, 115, A112245, doi:10.1029/2010JA015755.
- Lyon, J. G., J. A. Fedder, and C. M. Mobarry (2004), The Lyon–Fedder–Mobarry (LFM) global MHD magnetospheric simulation code, *J. Atmos. Solar Terr. Phys.*, **66**(15), 1333, doi:10.1016/j.jastp.2004.03.020.
- Mann, I. R., A. N. Wright, K. J. Mills, and V. M. Nakariakov (1999), Excitation of magnetospheric waveguide modes by magnetosheath flows, J. Geophys. Res., 104(A1), 333.
- Mann, I. R., T. P. O'Brien, and D. K. Milling (2004), Correlations between ULF wave power, solar wind speed, and relativistic electron flux in the magnetosphere: solar cycle dependence, *J. Atmos. Solar Terr. Phys.*, **66**, 187, doi:10.1016/j.jastp.2003.10.002.
- Mann, I. R., et al. (2008), The upgraded CARISMA magnetometer array in the THEMIS era, *Space Sci. Rev.*, **141**(1-4), 413, doi:10.1007/s11214-008-9457-6.
- Mathie, R. A., and I. R. Mann (2000), A correlation between extended intervals of ULF wave power and storm-time geosynchronous relativistic electron flux enhancements, *Geophys. Res. Lett.*, 27(20), 3261.
- Mauk, B. H., N. J. Fox, S. G. Kanekal, R. L. Kessel, D. G. Sibeck, and A. Ukhorskiy (2013), Science objectives and rationale for the Radiation Belt Storm Probes mission, *Space Sci. Rev.*, 179(1-4), 3, doi:10.1007/s11214-012-9908-y.
- Ozeke, L. G., I. R. Mann, and I. J. Rae (2009), Mapping guided Alfv'en waves magnetic field amplitudes observed on the ground to equatorial electric field amplitudes in space, *J. Geophys. Res.*, 114, A01214, doi:10.1029/2008JA013041.
- Ozeke, L. G., I. R. Mann, K. R. Murphy, I. J. Rae, D. K. Milling, S. R. Elkington, A. A. Chan, and H. J. Singer (2012), ULF wave derived radiation belt radial diffusion coefficients, *J. Geophys. Res.*, 117(A4), A04221, doi:10.1029/2011JA017335.
- Perraut, S., R. Gendrin, P. Robert, A. Roux, C. de Villedary, and D. Jones (1978), ULF waves observed with magnetic and electric sensors on GEOS-1, *Space Sci. Rev.*, 22, 347, doi:10.1007/BF00210873.

- Perry, K. L., M. K. Hudson, and S. R. Elkington (2005), Incorporating spectral characteristics of Pc5 waves into three-dimensional radiation belt modeling and the diffusion of relativistic electrons, *J. Geophys. Res.*, 110(A3), A03,215, doi:10.1029/2004JA010760.
- Press, W. H., S. A. Teukolsky, W. T. Vetterling, and B. P. Flannery (1992), Numerical recipes in Fortran 77: The art of scientific computing, Fortran Numerical Recipes, vol. 1, 2 ed., 922 pp., Cambridge Univ. Press, New York.
- Rae, I. J., I. R. Mann, K. R. Murphy, L. G. Ozeke, D. K. Milling, A. A. Chan, S. R. Elkington, and F. Honary (2012), Ground-based magnetometer determination of in situ Pc4–5 ULF electric field wave spectra as a function of solar wind speed, J. Geophys. Res., 117(A4), A04221, doi:10. 1029/2011JA017335.
- Ridley, A. J., G. Lu, C. R. Clauer, and V. O. Papitashvili (1998), A statistical study of the ionospheric convection response to changing interplanetary magnetic field conditions using the assimilative mapping of ionospheric electrodynamics technique, J. Geophys. Res., 103, 4023.
- Roederer, J. G. (1970), Dynamics of Geomagnetically Trapped Radiation, 166 pp., Springer-Verlag, New York.
- Rostoker, G., S. Skone, and D. N. Baker (1998), On the origin of relativistic electrons in the magnetosphere associated with some geomagnetic storms, *Geophys. Res. Lett.*, **25**, 3701.
- Ruohoniemi, J. M., and R. A. Greenwald (1998), The response of high-latitude convection to a sudden southward IMF turning, *Geophys. Res. Lett.*, 25, 2913.
- Russell, C. T. (Ed.) (1995), *The Global Geospace Mission*, Kluwer Academic, Boston, (reprinted from *Space Sci. Rev.*, 71, nos 1–4, 1995).
- Sarris, T. E., et al. (2009a), Characterization of ULF pulsations by THEMIS, *Geophys. Res. Lett.*, 36(4), L04104, doi:10.1029/2008GL036732.
- Sarris, T. E., X. Li, and H. J. Singer (2009b), A long-duration narrowband Pc5 pulsation, J. Geophys. Res., 114, A01213, doi:10.1029/2007JA012660.
- Sarris, T. E., W. Liu, X. Li, K. Kabin, E. R. Talaat, R. Rankin, V. Angelopoulos, J. Bonnell, and K.-H. Glassmeier (2010), THEMIS observations of the spatial extent and pressure-pulse excitation of field line resonances, *Geophys. Res. Lett.*, 37, L15104, doi:10.1029/2010GL044125.
- Sarris, T. E., X. Li, W. Liu, E. Argyriadis, and R. Ergun (2012), Mode number calculations of ULF field line resonances using ground magnetometers and THEMIS measurements, *J. Geophys. Res. Space Physics*, **118**, 6986–6997, doi:10.1002/2012JA018307.
- Schulz, M. (1996), Canonical coordinates for radiation-belt modeling, in *Radiation Belts: Models and Standards*, vol. 97, edited by J. F. Lemaire, D. Heynderickx, and D. N. Baker, p. 153, AGU, Washington, D.C.
- Schulz, M., and L. J. Lanzerotti (1974), Particle Diffusion in the Radiation Belts, Physics and Chemistry in Space, 7, 215 pp., Springer-Verlag, New York.
- Shprits, Y. Y., and R. M. Thorne (2004), Time dependent radial diffusion modeling of relativistic electrons with realistic loss rates, *Geophys. Res. Lett.*, 31, L08805, doi:10.1029/2004GL019591.
- Shprits, Y. Y., R. M. Thorne, G. D. Reeves, and R. Friedel (2005), Radial diffusion modeling with empirical lifetimes: comparison with CRRES observations, *Ann. Geophys.*, **23**(4), 1467.
- Shprits, Y. Y., R. M. Thorne, R. Friedel, G. D. Reeves, J. Fennell, D. N. Baker, and S. G. Kanekal (2006), Outward radial diffusion driven by losses at magnetopause, *J. Geophys. Res.*, 111, A11,214, doi:10.1029/2006JA011657.
- Shprits, Y. Y., S. R. Elkington, N. P. Meredith, and D. A. Subbotin (2008), Review of modeling of losses and sources of relativistic electrons in the outer radiation belt I: Radial transport, *J. Atmos. Solar Terr. Phys.*, 70(14), 1679, doi:10.1016/j.jastp.2008.06.008.

- Shprits, Y. Y., D. Subbotin, and B. Ni (2009), Evolution of electron fluxes in the outer radiation belt computed with the VERB code, J. Geophys. Res., 114(A11), A11209, doi:10.1029/2008JA013784.
- Sibeck, D. G., and V. Angelopoulos (2008), THEMIS science objectives and mission phases, *Space Sci. Rev.*, 141, 35, doi:10.1007/s11214-008-9393-5.
- Singer, H., L. Matheson, R. Grubb, A. Newman, and D. Bouwer (1996), Monitoring space weather with the GOES magnetometers, *Proc. SPIE*, 2812, 299, doi:10.1117/12.254077.
- Singer, H. J., W. P. Sullivan, P. Anderson, F. Mozer, P. Harvey, and J. Wygant (1992), Fluxgate magnetometer instrument on CRRES, J. Spacecr. Rockets, 29, 599.
- Southwood, D. J., J. W. Dungey, and R. J. Etherington (1969), Bounce resonant interaction between pulsations and trapped particles, *Planet. Space Sci.*, 17, 349.
- Sturrock, P. A. (1994), Plasma Physics, 335 pp., Cambridge Univ. Press, Cambridge.
- Takahashi, K., C. T. Russell, and R. R. Anderson (1985), ISEE 1 and 2 observations of the spatial structure of a compressional Pc 5 wave, *Geophys. Res. Lett.*, 12, 613.
- Tu, W., S. R. Elkington, X. Li, W. Liu, and J. Bonnell (2012), Quantifying radial diffusion coefficients of radiation belt electrons based on global MHD simulation and spacecraft measurements, J. Geophys. Res., 117, A10210, doi:10.1029/2012JA017901.
- Tu, W., G. S. Cunningham, Y. Chen, M. G. Henderson, E. Camporeale, and G. D. Reeves (2013), Modeling radiation belt electron dynamics during GEM challenge intervals with the DREAM3D difusion model, J. Geophys. Res., 118(10), 6197, doi:10.1002/jgra.50560.
- Turner, D. L., V. Angelopoulos, Y. Shprits, A. Kellerman, P. Cruce, and D. Larson (2012), Radial distributions of equatorial phase space density for outer radiation belt electrons, *Geophys. Res. Lett.*, **39**(9), L09101, doi:10.1029/2012GL051722.
- Wygant, J. R., P. R. Harvey, D. Pankow, F. S. Mozer, N. Maynard, H. Singer, M. Smiddy, W. Sullivan, and P. Anderson (1992), CRRES electric field/Langmuir probe instrument, *J. Spacecr. Rockets*, 29, 601.